Atmospheric sounding using IASI
1st Year Report

Lucy Ventress
AOPP, University of Oxford

August, 2010

Contents

Chapter 1

Introduction

Atmospheric observations are vital in the process of weather forecasting. (It is only with a large range of observational data monitoring the Earth's atmosphere, land and ocean that forecasts can be produced.) Presently observations come from several sources: radiosondes, surface data, aircraft observations and satellites. Satellites have become the most prevalent source of information due to the quantity of data they produce, providing measurements of atmospheric properties such as pressure, temperature, humidity and wind with almost global coverage

Although satellites provide almost global coverage, there are still areas that are rarely or never observed. To overcome this problem the process of data assimilation is used. This involves combining the observations available with a forecast of what the conditions are expected to be to form a best estimate of the current state of the atmosphere. This best estimate, or analysis, is the starting point for numerical weather forecasts, which simulate the Earth's atmospheric processes that can affect the weather.

Infrared sounding instruments, such as the Infrared Atmospheric Sounding Interferometer (IASI), which will be discussed in chapter 2, can provide data with high spectral resolution but only in cloud free areas. Currently, to see below the cloud top, microwave instruments are needed. A large number of weather centres now use the spectral data from IASI and its use has been shown to have a significant positive impact on global Numerical Weather Prediction (NWP). This impact became apparent shortly after IASI's launch despite its data initially having a fairly conservative weighting during the assimilation process [1]. Its radiometric accuracy has been shown through comparisons with data from AIRS (Atmospheric InfraRed Sounder) and AATSR (Advanced Along-Track Scanning Radiometer) at 11 microns, in both cases agreement being better than 0.1 K, [2] [3].

Radiative Transfer models are used to simulate observations and are a fundamental part in the retrieval of atmospheric compounds. Two models available for use are described in chapter 3. One of the essential inputs into the models is a reliable spectroscopic database that contains accurate line shapes and positions as well as many other active atmospheric gas parameters. There are several databases to choose from including the HIgh-resolution TRANsmission molecular absorption database (HITRAN) and Gestion et Etude des Informations Spectroscopiques Atmosphériques (GEISA) databases. These are updated regularly as new research is carried out, for example the addition of new water vapour lines in the HITRAN database [4] and the improved nitric acid, HNO_3, parameters in the GEISA database [5]. The impact of these updates is assessed in chapter 4.

IASI measures the radiance emitted from the Earth and atmosphere. In a cloud free region the radiance can be measured throughout the atmosphere. This allows vertical information to be derived for certain species, assuming surface parameters such as temperature and emissivity and the atmospheric temperature are known. If a species is optically thin a total column amount can be retrieved, whereas for species that are optically thick it may be possible to retrieve a full vertical profile [6]. Chapter 5 examines which gases may be retrieved as a profile and which as a total column, and the errors associated with such a retrieval.

Another topic discussed in chapter 5, that currently requires further research, is channel selection. Although the number of IASI's spectral channels used in NWP has increased since its launch, the maximum is still at approximately 200 channels. The majority of these lie in the long wave CO_2 band and provide atmospheric temperature information, whilst the IASI water vapour band is currently under used. Only a fews tens of the water vapour channels are assimilated. Reasons suggested for this limited use include difficulties with the observation error correlations and biases in the assimilating NWP models [1].

Principal Component Analysis (PCA) is a method of projecting spectra onto a principal component basis and is being explored for use in data compression. The method of PCA is described in chapter 6 along with an example. Principal Component Compression (PCC) has shown powerful properties of noise filtering whilst minimizing the loss of information on trace gases and species, and a strong compression rate [7]. It is planned that, in the near future, the compressed PC spectra will be disseminated in parallel with the full IASI radiance spectra. However, attention must be paid to ensure that all relevant information is kept and also that certain events, such as biomass burning or pollutant plumes, are not missed. This depends upon similar features being included in the 'training set' of spectra used to create the PCs and the number of PCs chosen for compression. It remains to be investigated whether or not trace gas retrievals can benefit from the increased signal to noise ratio in the reconstructed radiances and if the PC scores will contain enough information for applications such as chemistry monitoring or if the full IASI spectra will be needed.

Most NWP centres only assimilate data that is cloud free. However, this wastes a large proportion of the total observations. Work is currently being done by several meteorological groups, for example ECMWF [8], Météo France [9] and the UK Met Office [10], to include cloud-affected radiances in the assimilation. Many cloud characterisation schemes use the CO_2-slicing method to obtain cloud parameters such as cloud top height and the net emissivity, and assume a single layer of cloud. It is hoped that future work will lead to a more realistic description of cloud conditions. Current improvements include using only homogeneous overcast conditions or only using data above clouds, by selecting channels with sensitivity down to the cloud top height. However, at present, inter-comparisons of cloud products are showing large differences. More validation and comparisons are needed to assess the quality of the operational products. With the AVHRR instrument onboard the same satellite platform as IASI, improvements in the coupling of the data from both instruments could lead to improved results.

Contained in this report is the work carried out during the first year of my study, primarily learning and implementing the tools I will need throughout my future research.

Chapter 2

The Infrared Atmospheric Sounding Interferometer

The Infrared Atmospheric Sounding Interferometer (IASI) is one of eleven instruments onboard the METOP-A satellite that was launched on 19$^{\text{th}}$ October 2006. It was developed by CNES (Centre National d'Etudes Spatiales) for use as part of the EUMETSAT (European Organisation for the Exploitation of Meteorological Satellites) European Polar system. Two more instruments in the same series of satellites are planned to be mounted on METOP-B and METOP-C, due to be launched in 2012 and 2016 respectively, allowing the IASI instrument to provide observations and measurements over a long timescale.

The IASI instrument is an infrared Fourier transform spectrometer associated with an imaging system, which uses nadir viewing geometry passively to measure the radiance from Earth. The radiation emitted from both Earth and the atmosphere is affected by the emission, absorption and scattering of the atmospheric molecules along its optical path. It is the radiation resulting from these interactions that IASI measures as the atmospheric spectrum, containing thousands of emission/absorption features [11]. The instrument is based on a Michelson interferometer; this decomposes the emitted spectrum, after which an inverse Fourier transform and radiometric calibration are applied. The calibrated data are subsequently transmitted to the ground segment [12]. The essential components of the instrument are discussed in detail elsewhere, [12] [13] [14] [15], but include:

- A scanning mirror.
- An afocal telescope to transfer the image onto the scan mirror.
- The Michelson interferometer, including a beamsplitter and corner cube mirrors that are designed to create the optical path difference necessary for the specified spectral resolution.
- The cold box, which the recombined beams are directed into, contains refractive optics that divides the spectral range into three bands.
- The Digital Processing Subsystem that carries out the inverse Fourier transform and calibration on the interferograms before being transmitted to the ground.

The main characteristics of the IASI instrument are summarised in Table 2.1, taken from Clerbaux *et al.* [17]. IASI covers the spectral range 645–2760 cm^{-1} with a spectral resolution of 0.5 cm^{-1} (apodized) giving a total of 8461 channels in each IASI spectrum. This results in a large quantity of data that can cause problems for both retrievals and data assimilation. Choosing an optimal subset of the channels is an established method to reduce the amount of data and is discussed in section 5.2.1, [18]. The spectral range is divided into three bands as shown in figure 2.3. 'Band 1', from 645–1210 cm^{-1}, is primarily for temperature and ozone sounding, 'Band 2',

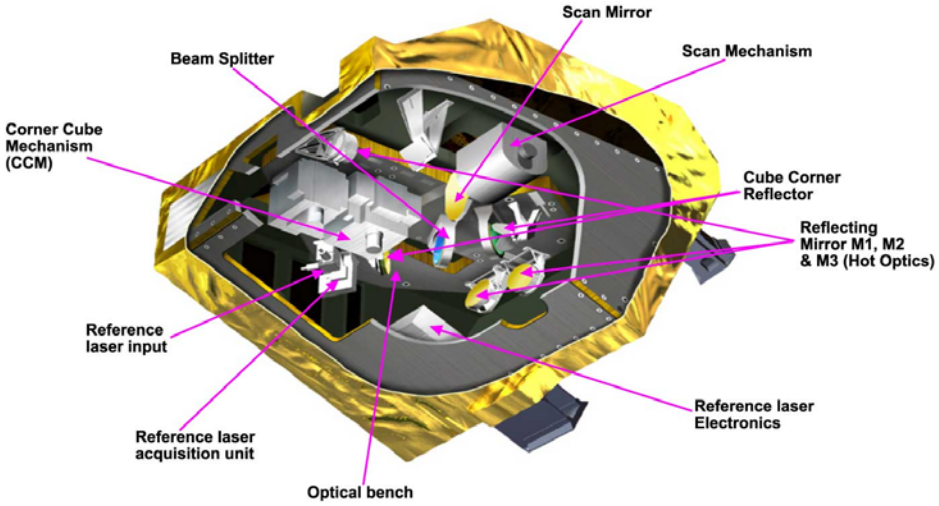

Figure 2.1: An internal view of IASI components - View 1. (Picture by CNES, [16])

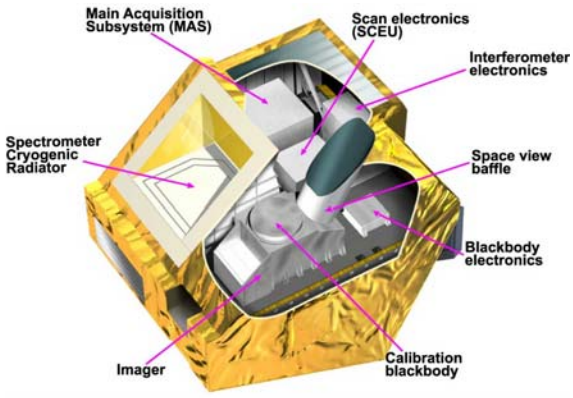

Figure 2.2: An internal view of IASI components - View 2. (Picture by CNES, [16])

from 1210–2000 cm^{-1}, is primarily for water vapour sounding and retrieving N_2O and CH_4 column amounts and 'Band 3', from 2000–2760 cm^{-1}, is for temperature sounding and the retrieval of N_2O and CO column amounts [19].

IASI achieves global coverage and provides measurements twice a day at each location, at a local time of 09:30, from a low altitude, sun synchronous orbit. The instrument scans perpendicularly to the motion of the satellite between angles $-47.85°$ and $+47.85°$, with respect to the nadir. Within each scan there are 30 steps at which measurements are taken, as well as views to the calibration targets, an internal hot black body and cold deep space. Each view consists of a 2×2 matrix containing independent circular pixels with diameters of 12 km, as shown in figures 2.4a and 2.4b, to increase the probability of obtaining cloudfree views. The IASI scan pattern provides measurement locations compatible with other instruments onboard the METOP satellite [13].

Table 2.1: IASI Instrumental Characteristics

	Characteristics
Spectral Range	645–2760 cm^{-1} (15.5–3.62 μm)
Spectral Resolution	0.5 cm^{-1} (apodized)
Instrumental Noise	0.2 to 0.35 K (NEDT at 280 K)
Pixel Size	Diameter of 12 km, 4 pixels matrix, across-track scanning
Data Rate	1.5 megabits per second
Lifetime	5 years
Altitude	$\sim$ 817 km
Orbit	polar sun-synchronous
Inclination	98.7 ° to the equator
Local time	$\sim$ 09:30
Orbital Period	101 min

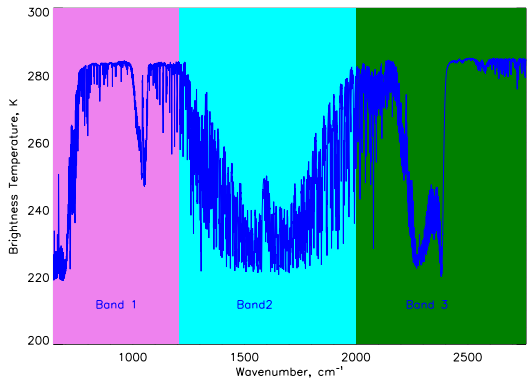

Figure 2.3: A typical IASI spectrum and its spectral bands

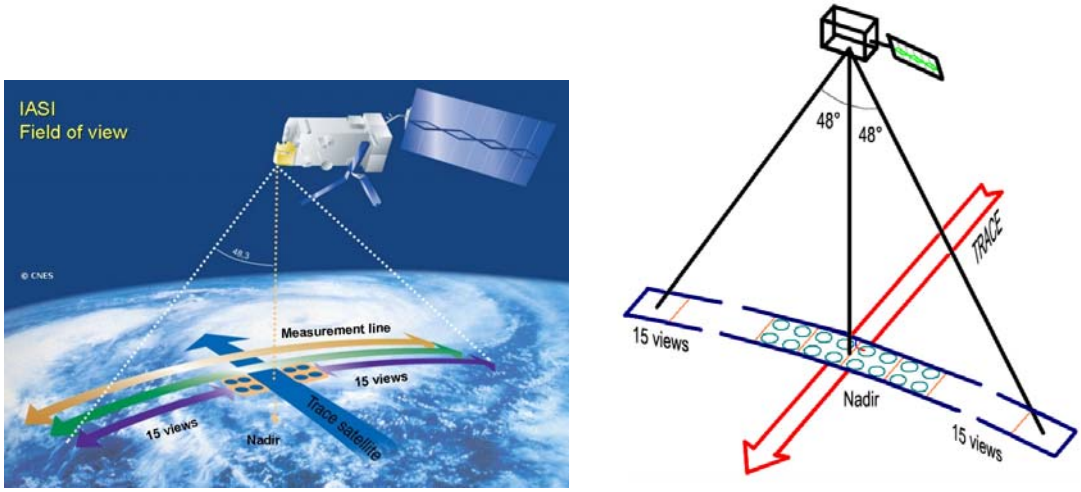

Figure 2.4: The IASI field of view. (Pictures by CNES, [16])

Chapter 3

Radiative Transfer Models

3.1 Radiative Transfer

The equation of radiative transfer describes how radiation propagating through the atmosphere is both attenuated, due to absorption and scattering, and enhanced by thermal emission. This forms the basis for modelling atmospheric radiances and interpreting remote sensing measurements.

Consider a beam of radiation passing through a layer of the atmosphere containing an absorbing (or scattering) gas, of thickness dz. The fractional decrease in radiance, L_ν, for a given wavenumber, ν, is given by Lambert's Law [20],

$$d\mathrm{L}_\nu = -k_\nu(z)\rho_a(z)\mathrm{L}_\nu(z)dz, \tag{3.1}$$

where ρ_a is the density of the gas and hence $\rho_a dz$ gives the mass of gas in the beam, assuming unit cross-sectional area. The constant of proportionality is k_ν, the extinction coefficient, which is the sum of the absorption and scattering coefficients defining their respective contributions to $d\mathrm{L}_\nu$.

The layer of atmosphere will also be emitting radiation, the amount depending upon its temperature. Assuming thermodynamical equilibrium and no scattering, Kirchoff's Law can be applied and the emitted radiation becomes

$$d\mathrm{L}_\nu = k_\nu(z)\rho_a(z)\mathrm{J}_\nu(z)dz \tag{3.2}$$

where $\mathrm{J}_\nu(z)$ is the source function, which is assumed to be the Planck black body function, $\mathrm{B}_\nu(T)$, [21]. Combining both extinction and emission, the radiative transfer equation (or Schwarzschilds's equation), is obtained

$$\frac{d\mathrm{L}_\nu}{dz} = -k_\nu\rho_a(\mathrm{L}_\nu - \mathrm{B}_\nu(\mathrm{T})). \tag{3.3}$$

Using the plane-parallel approximation and integrating this equation from a source point, z_s, to an observation point, z_{obs} leads to the integral equation of transfer

$$\mathrm{L}_\nu(z_{obs}) = \mathrm{L}_\nu(z_s)\tau_\nu(z_s, z_{obs}) + \int_{z_s}^{z_{obs}} \mathrm{B}_\nu(T(z))\frac{d\tau}{dz}dz, \tag{3.4}$$

where τ is the transmittance between z_s and z_{obs} and

$$\tau(z_s, z_{obs}) = \exp\left(-\int_{z_s}^{z_{obs}} k_\nu(z)\rho_a(z)dz\right). \tag{3.5}$$

Solving equation 3.4 is the main aim of radiative transfer models [22].

During this study, brightness temperature has been worked with instead of radiance. Brightness temperature, T_b, is the temperature a black body is expected to have for a given radiance at a particular wavenumber:

$$\mathrm{T}_\mathrm{b}^{-1} = \frac{\mathrm{k}}{\mathrm{hc}\nu}\ln\left(1 + \frac{2\mathrm{hc}^2\nu^3}{\mathrm{L}_\nu}\right) \tag{3.6}$$

where h is the Plank constant, c is the speed of light anf k is the Boltzmann constant.

3.2 Radiative Transfer Models

Radiative transfer models attempt to calculate accurate top of atmosphere radiances, given atmospheric profiles of the gases present. As mentioned in section 3.1, their aim is to solve the equation of radiative transfer. The spectrum is calculated as a set of radiances at each spectral point on a chosen grid. This is convolved with the channel's corresponding spectral response function to obtain the simulated radiance expected from a particular instrument.

A spectral grid is chosen and the atmosphere divided into horizontal layers [23], which are assumed to be homogeneous. These layers may be of equal or varying widths and given in either height or pressure co-ordinates. For each layer, characteristic values are determined for its temperature, pressure and the concentrations of the atmospheric gases present that should give the same transmittance values as the 'real' inhomogeneous layer. These quantities allow the calculation of the emission and absorption coefficients, the essential components under local thermodynamic equilibrium.

There are two main types of radiative transfer models: line by line radiative transfer models and fast radiative transfer models. Although line by line models produce much more accurate results they are very computer processing heavy and cannot be run in near real time. For this reason, fast radiative transfer models were developed for use in numerical weather prediction. In the following sections, two models are discussed explaining how each works and their differences.

3.2.1 Reference Forward Model

The Reference Forward Model, or RFM, is a line by line model developed at the University of Oxford [24]. It is based on the line by line model GENLN2 [22] and was developed originally for use with the Michelson Interferometer for Passive Atmospheric Sounding, MIPAS, but has since been developed into a general purpose code for many spectroscopic calculations. Line by line models perform accurate calculations of atmospheric radiances and transmittance at high spectral resolution.

The line by line model first calculates the monochromatic absorption coefficient, $k(\nu)$, at wavenumber ν for every spectral line using the parameters supplied by a database containing spectroscopic parameters. The line strengths and widths read in at standard temperature and pressure must be adjusted to the temperature and pressure of the path through the atmosphere. The absorption coefficient at wavenumber ν can be expressed as the sum of the contributions to absorption from all spectral lines, i, in range, i.e.

$$k(\nu)_j = \Sigma_i \, S_{ij} \, g(\nu - \nu_i)_j, \tag{3.7}$$

where S_{ij} is the strength of line i adjusted to local path conditions and $g(\nu - \nu_i)_j$ is the line shape function. The Voigt profile shape, which is a convolution of the Lorentz and Doppler line shapes, is appropriate to use in most atmospheric transmittance cases.

The actual line by line calculation comes from the calculation of transmittances over the specified spectral range for each gas, in a specified number of atmospheric layers. The total transmittance, from equation 3.5, can be approximated as

$$\tau(\nu) = \exp(-\Sigma_j \, k(\nu)_j \, u_j), \tag{3.8}$$

$$= \exp(-\chi(\nu)), \tag{3.9}$$

where $\chi(\nu)$ is the optical depth and u_j is the amount of absorber in the atmospheric path, j. The total optical depth can be calculated as the sum of the optical depths of each individual path, and the transmittance can subsequently be evaluated. When dealing with multiple absorbers, Beers Law can be applied and the total transmittance becomes the product of the transmittances of each

absorber; i.e. $\tau_{\rm n} = \tau_1\tau_2\tau_3\ldots\tau_n$, where n is the number of absorbers.. This now allows the latter part of equation 3.4 to be solved and the radiance at each observation point can be calculated:

$$\mathrm{R}_\nu(z_{obs}) = \int_\nu \int_{z_s}^{z_{obs}} \mathrm{B}_\nu(T(z))\frac{d\tau}{dz}dz\phi(\nu)d\nu, \tag{3.10}$$

where $\phi(\nu)$ is the instrument spectral response function. This process is explained in greater detail in the GENLN2 User Guide [22].

3.2.2 RTTOV

The RTTOV model is the Radiative Transfer model for TOVS, where TOVS is the Television InfraRed Observation Satellite (TIROS-N) Operational Vertical Sounder (TOVS). It was originally developed at ECMWF for use with TOVS but, as with the RFM, has subsequently been developed and adapted for use with other instruments. The latest version is RTTOV-9 [25], which includes all the scientific features of the fast Radiative Transfermodel for IASI, RTIASI [19], a model developed for pre-launch simulation studies of IASI data.

In RTTOV the transmittances are not calculated as described for the RFM, rather they are expressed as a function of profile dependent predictors as explained by Matricardi, 2009 [26]. This form of calculation increases the computer efficiency allowing the model to be used in near real time to monitor and assimilate satellite radiances as is needed for numerical weather prediction.

For given atmospheric profiles and parameters the effective optical depth, $\sigma^{\rm eff}_{j,\nu}$ (or convolved transmittance, $\hat{\tau}_{j,\nu} = \exp(-\sigma^{\rm eff}_{j,\nu})$), becomes a function of profile dependent predictors and expansion coefficients (or fast transmittance coefficients), which depend upon temperature, absorber amount, pressure and viewing angle [27]. For the layer from pressure level j to space

$$\sigma^{\rm eff}_{j,\nu} = 0, \quad j = 1 \tag{3.11}$$

$$\sigma^{\rm eff}_{j,\nu} = \sigma^{\rm eff}_{j-1,\nu} + \sum_{k=1}^{M} a_{j-1,\nu,k}X_{k,j-1}, \quad j = 2, l \tag{3.12}$$

where the functions $X_{k,j}$ are the profile dependent predictors of the model and M is the number of them. The regression coefficients, $a_{j-1,\nu,k}$, are derived from accurate line by line calculated transmittances for each atmospheric level, where the input to the line by line model is a training set of atmospheric profiles specifically chosen to represent variations found in the atmosphere. The predictors' functional dependence are on factors such as the spectral region and the absorbing gas and are are calculated from profile variables. The profile variables are defined from ratios of reference temperature, water vapour and ozone profiles. Currently the predictors for use with RTTOVs are calculated using the Line-By-Line Radiative Transfer Model, LBLRTM [28]. The calculations and variables are explained in detail in Matricardi and Saunders, [19] and Matricardi *et al.*, [27].

The radiance calculation, which differs from the RFM calculation, can now be carried out. The difference arises from the use of spectrally averaged transmittances and Planck function. The calculation, in this case, is only a single integration over the atmospheric path:

$$\mathrm{R}(z_{obs}) = \int_{z_s}^{z_{obs}} \bar{\mathrm{B}}(T(z))\frac{d\bar{\tau}}{dz}dz, \tag{3.13}$$

where $\bar{\mathrm{B}} = \int_\nu \mathrm{B}\phi d\nu$ and $\bar{\tau} = \int_\nu \tau\phi d\nu$. This allows the model to be fast and can therefore be implemented in real time data assimilation. Information can however be lost through the assumptions made.

Chapter 4

Spectroscopic Database Comparison

4.1 Introduction

Spectroscopic databases are an essential input into forward models used in radiative transfer calculations. The simulation of recorded radiance spectra from instruments, such as IASI, depends upon the accuracy of the known active atmospheric gas parameters. Such databases contain many components used in radiative transfer calculations; for example, individual line parameters for molecules in the gas phase, absorption cross-sections for molecules in which the individual lines cannot be resolved and refractive indices [29]. However, only the line parameters are investigated in this chapter. There are several databases to choose from and they are updated at regular intervals as new research is carried out. The databases do not contain exactly the same data, hence, the same results may not be returned from a radiative transfer model when using a different one. In this chapter a selection of the available spectroscopic databases are compared to discover if there are any molecules for which there are large discrepancies. The databases compared are:

1. HITRAN 2000, [30]
2. HITRAN 2004, [31]
3. HITRAN 2008, [29]
4. GEISA 2003, [32]
5. GEISA-IASI 2009, [33]
6. MIPAS, [34]

where 1, 2 and 3 are versions of HITRAN (HIgh-resolution TRANsmission molecular absorption database), 4 and 5 are versions of GEISA (Gestion et Etude des Informations Spectroscopiques Atmosphériques), and the MIPAS (Michelson Interferometer for Passive Atmospheric Sounding) database [34] is a customised version of the HITRAN databases made specifically for use with the MIPAS instrument.

The spectral range used, 645 –2760 cm^{-1}, is that of the IASI instrument as this is the main instrument of study; however, the results are applicable for all instruments. The spectral resolution, 0.1 cm^{-1}, was chosen so that as much detail of the spectrum could be examined as possible. The forward model used to simulate the spectra was the Reference Forward Model (RFM) [24] developed at AOPP, Oxford University and the molecules considered were the standard HITRAN line molecules as listed on the HITRAN website [35]. Any molecules requiring cross-section data were excluded. A mid-latitude daytime atmospheric profile was used to calculate the molecular concentrations.

The RFM requires its input files to be in a binary format. HITRAN files are downloaded in an ASCII format and must be converted into an RFM compatible binary file. This is done using the FORTRAN program 'hitbin.f' that can be found in the RFM User's Manual [24]. The GEISA databases are in another format and must first be converted to an ASCII file using the Fortran program 'geihit.f' before also being converted into a binary format using the 'hitbin.f' program.

Transmittance, τ, as defined in section 3.1, is the fraction of radiation, at a given wavenumber, that passes through the atmosphere along a path being neither absorbed nor scattered. The absorption, A, is the fraction of radiation, at a given wavenumber, that is absorbed along a path. Assuming negligible scattering, $\tau = 1 - A$. Optical depth, χ, is a measure of how opaque a medium is to radiation and how much the beam is attenuated through absorption by molecules. It can be expressed by the equation $\chi = -\ln \tau$.

For each database considered, the optical depth spectra were calculated for each molecule using the RFM. Each molecule's spectrum was calculated assuming that only that molecule was present in the atmosphere. Presented in the following section are the findings from the comparisons. Although a full survey of all 'line' molecules was performed only the results for the major absorbers are shown. For full details of all molecules see 'Comparing Spectroscopic Databases' [36]. The reference database used in comparisons is HITRAN 2004.

For each molecule we show:

- The optical depth spectra for all databases,
- The absolute difference in optical depth between each database and HITRAN 2004 (only differences greater than 10^{-3} were considered).

If the absolute values of the optical depth are greater than 10^{-3} we also plot:

- The percentage difference in optical depth between each database and HITRAN 2004,
- The absolute difference in absorption between each database and HITRAN 2004. This has been included as it is more closely related to the expected difference in top of atmosphere radiance than the optical depth.

4.2 Main Gases

4.2.1 Carbon Dioxide, CO_2

The discrepancies between HITRAN 2000 and HITRAN 2004 that can be seen in figure 4.1c between 650–1100 $cm^{-1}$and also between 2000–2400 cm^{-1} are due to an update in line positions in HITRAN 2004 shown in Table 8 of Rothman et al., 2005 [31]. The visible differences in the spectra produced by HITRAN 2004 and 2008 in figure 4.1a are caused by the intensity cutoff applied to the HITRAN databases being lowered to 4×10^{-30} for HITRAN 2008, as described by Rothman et al., 2005, allowing the appearance of these weak bands. However the differences are of $O(10^{-6})$ and therefore insignificant. The difference between HITRAN 2000 and HITRAN 2004 around 2350 cm^{-1} shows a shift in the line position to a lower wavenumber in 2004. The same shift, although smaller, occurs in both GEISA 2003 and MIPAS. The differences in absorption between HITRAN 2004 and MIPAS appear to be due to shifts in line position.

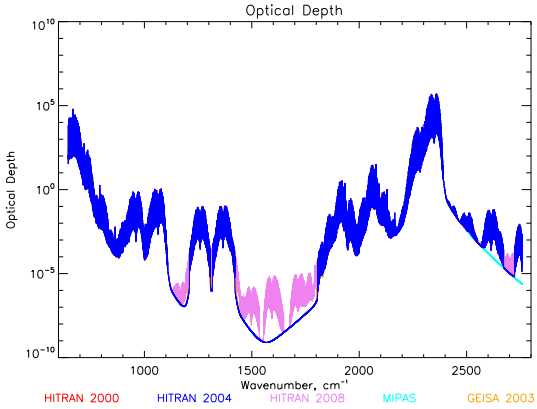

(a) Optical depth in each spectroscopic database

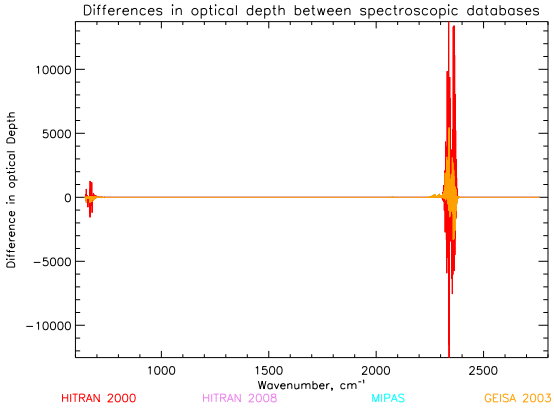

(b) Absolute difference in optical depth between each spectroscopic database and HITRAN 2004

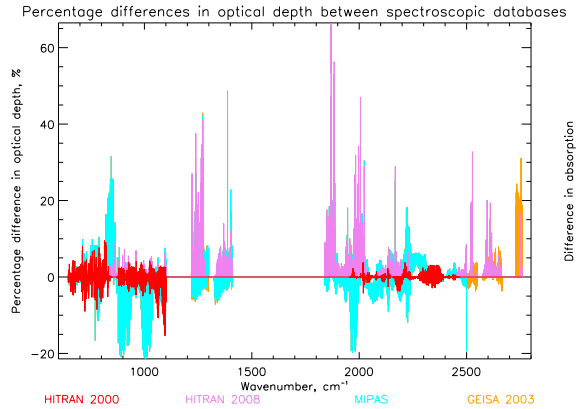

(c) Percentage difference in optical depth between each spectroscopic database and HITRAN 2004

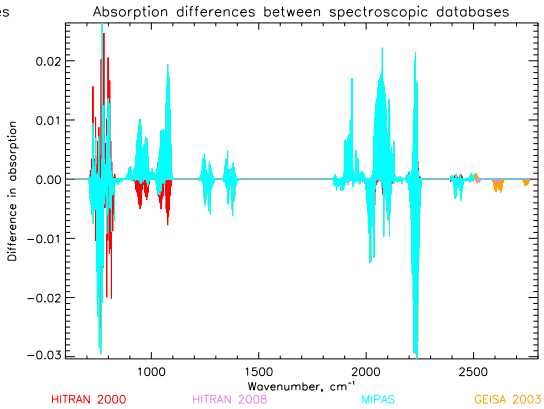

(d) Difference in absorbtion between each spectroscopic database and HITRAN 2004

Figure 4.1: CO2

4.2.2 Carbon Monoxide, CO

The same shift in line position exists between HITRAN 2004 and all the other databases except HITRAN 2008 in the band 2050–2250 cm^{-1}.

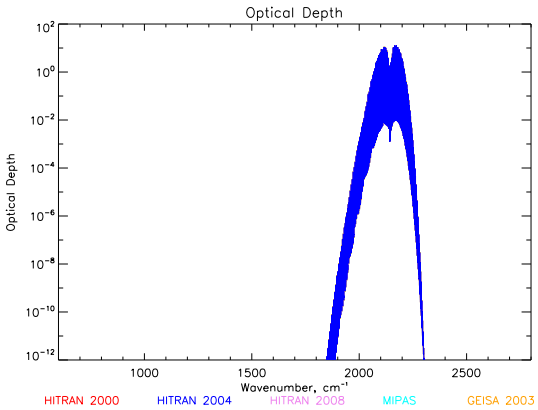

(a) Optical depth in each spectroscopic database

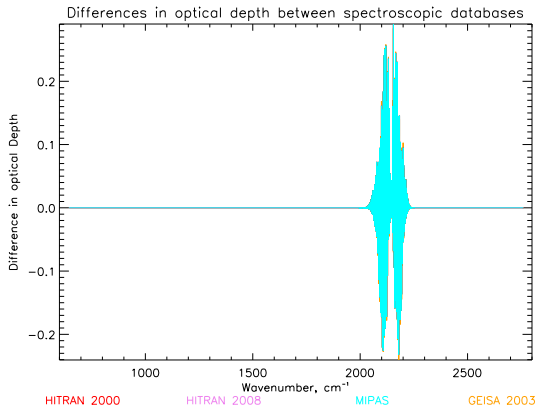

(b) Absolute difference in optical depth between each spectroscopic database and HITRAN 2004

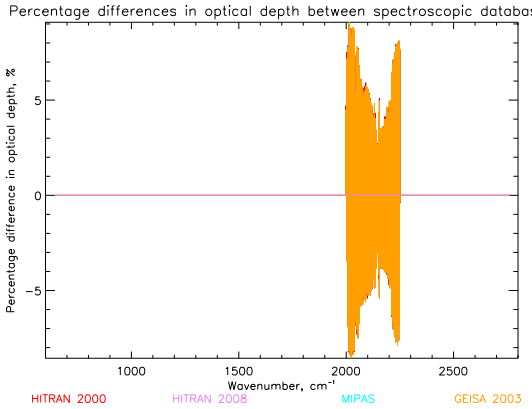

(c) Percentage difference in optical depth between each spectroscopic database and HITRAN 2004

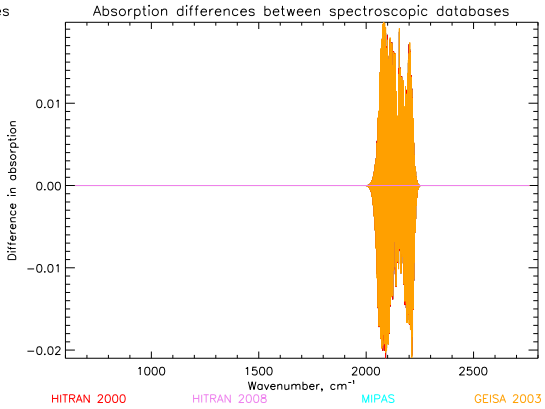

(d) Difference in absorbtion between each spectroscopic database and HITRAN 2004

Figure 4.2: CO

4.2.3 Ozone, O_3

A noticeable negative change in the optical depth of ozone can be observed in figure 4.3b when comparing the HITRAN 2000 and HITRAN 2004 data. There is also a difference when comparing HITRAN 2004 to both GEISA databases, where GEISA is lower in strength. In figure 4.3c the differences between HITRAN 2004 and HITRAN 2000 in the 1600 cm^{-1} and 2200 cm^{-1} range could be accounted for by the addition of nine new spectral bands to HITRAN 2004 that are not present in HITRAN 2000. The consistent difference between these two databases may also be due to the intensities of all the other bands having been divided by 1.04 in HITRAN 2004 as described in Rothman et al., 2005 [31].

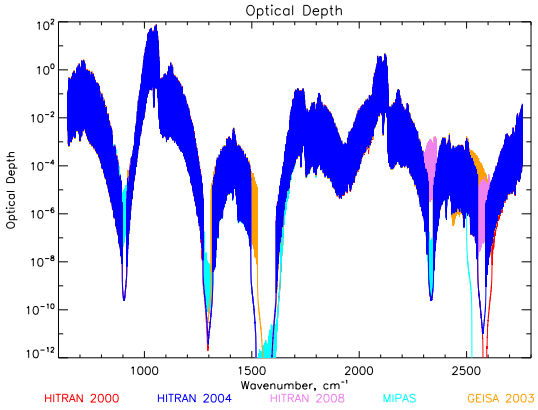

(a) Optical depth in each spectroscopic database

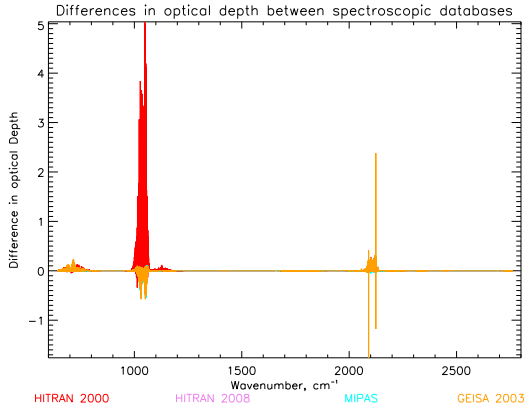

(b) Absolute difference in optical depth between each spectroscopic database and HITRAN 2004

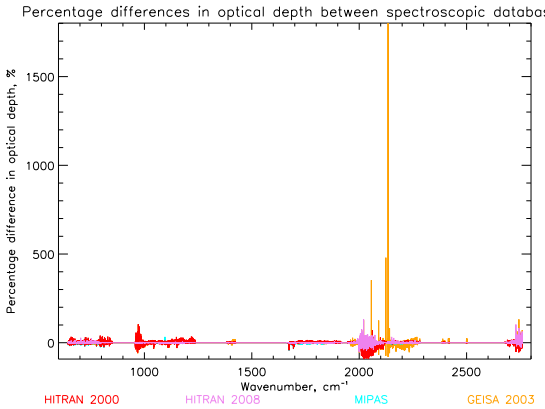

(c) Percentage difference in optical depth between each spectroscopic database and HITRAN 2004

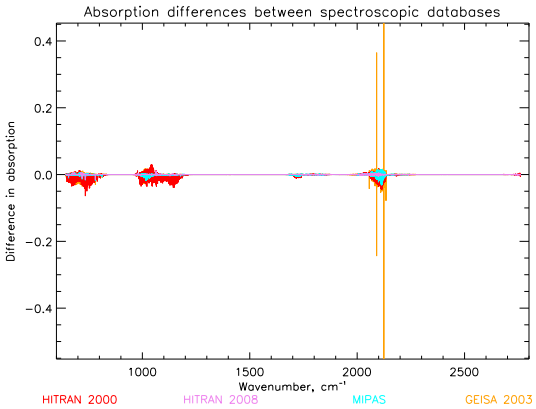

(d) Difference in absorbtion between each spectroscopic database and HITRAN 2004

Figure 4.3: O3

4.2.4 Water vapour, H_2O

The largest differences in figure 4.4b occur in the region 1300–2000 cm^{-1} where there is a decrease in line strength in HITRAN 2004 compared to that of HITRAN 2008, GEISA-IASI 2009 and MIPAS and a slight broadening of the Lorentz width in comparison to HITRAN 2000 and GEISA 2003. However when considering percentage differences, in figure 4.4c, the largest discrepancies are above 2500 cm^{-1}. There is a large increase in line strength in HITRAN 2004 compared to HITRAN 2000, and this is also clear when comparing the absorption in figure 4.4d. Many changes were made to HITRAN 2004, including an update for all positions and line intensities between 500 cm^{-1} and 8000 cm^{-1}, that may have caused the discrepancy. These are described in Rothman et al., 2005 [31]. There is also a large discrepancy between the GEISA databases and HITRAN above 2300 cm^{-1}.

In HITRAN 2008 the intensities within the 1000 cm^{-1} to 2000 cm^{-1} range were further updated having been underestimated by between 5% and 10%, [29]. These alterations agree with the result shown in figure 4.4c.

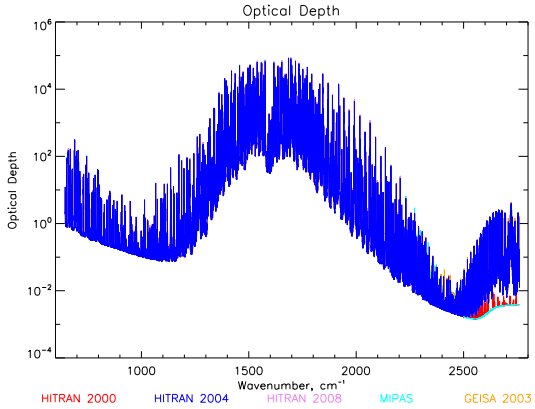

(a) Optical depth in each spectroscopic database

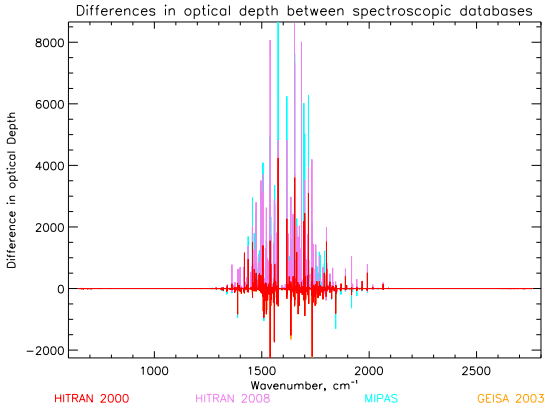

(b) Absolute difference in optical depth between each spectroscopic database and HITRAN 2004

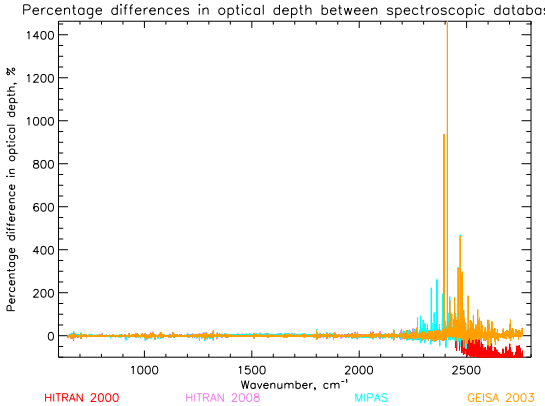

(c) Percentage difference in optical depth between each spectroscopic database and HITRAN 2004

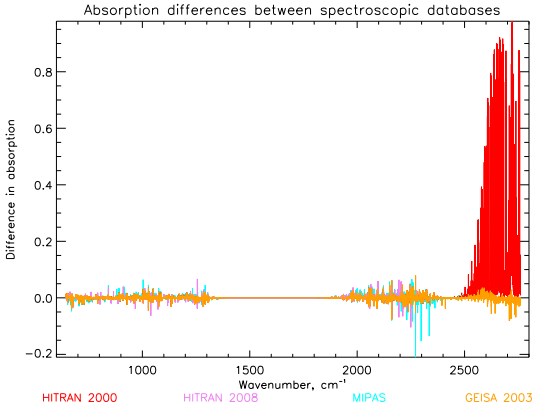

(d) Difference in absorbtion between each spectroscopic database and HITRAN 2004

Figure 4.4: H2O

4.2.5 Nitrous oxide, N_2O

Discrepancies between HITRAN 2000 and 2004 are due to a complete revision of all line intensities described by Rothman et al., 2005 [31].The strong line at 1167 cm^{-1} was absent in 2004 but was restored in 2008 [29]. However, the main differences between databases appear to be changes in the Lorentz widths that can be seen in figure 4.5b.

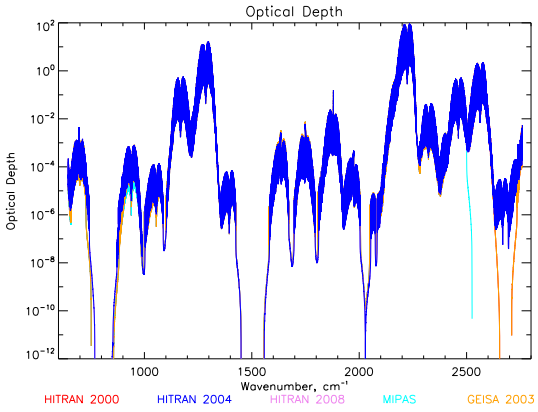

(a) Optical depth in each spectroscopic database

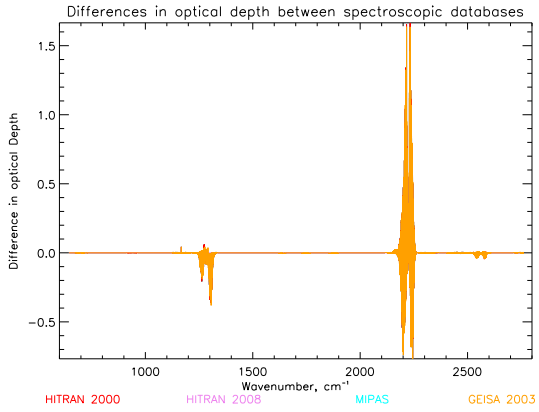

(b) Absolute difference in optical depth between each spectroscopic database and HITRAN 2004

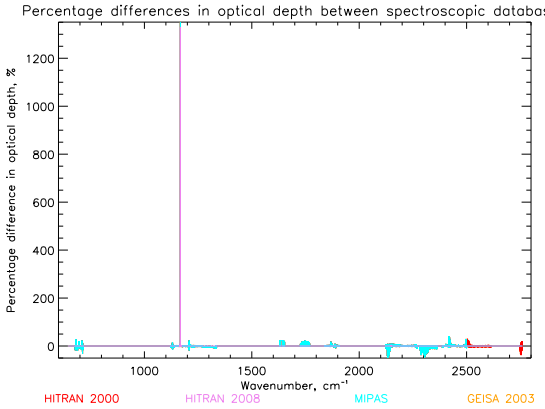

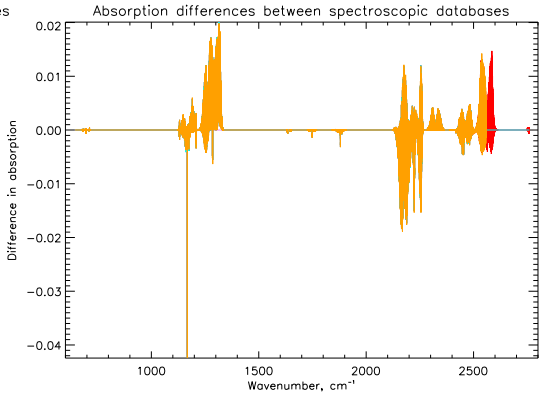

(c) Percentage difference in optical depth between each spectroscopic database and HITRAN 2004